مجلة جامعة بني وليد للعلوم الإنسانية والتطبيقية

تصدر عن جامعة بني وليد – ليبيا

Website: https://jhas-bwu.com/index.php/bwjhas/index

العدد التاسع والعشرون، 2023

A comparative study on the long-term microstructure of soil stabilisation with calcium and magnesium-based binders.

M. Ebailila[1*], J. Kinuthia[2], J. Oti[3], S. Attelisi[4],

[1,4] Department of Civil Engineering/Faculty of Engineering/Bani Waleed University, Libya

[2,3] Faculty of Computing, Engineering and Science/University of South Wales, UK

*Crosspnding author: mansour.ebailila@yahh.co.uk

تاريخ الاستلام: 14-06-2023 تاريخ القبول: 30-06-2023 تاريخ النشر: 07-09-2023

Abstract: Analytical and microstructure investigations such as x-ray diffraction (XRD), derivative thermogravimetric (DTG), and scanning electron microscopy (SEM) among others, are typically used by researchers to detect and quantify the amount of formed minerals including ettringite minerals in gypseous soil treated with lime or cement. However, the detection of ettringite crystals is sometimes difficult, suggesting that the appearance of ettringite under the microstructure analysis is also dependent on the curing and experimental procedure. Therefore, a series of soil mixtures designed by use of two different soils (pure kaolin soil and artificial gypseous kaolin soil) and stabilised with 10 wt% of lime-L, cement-C and MgO-M, were investigated using multi-scale investigations including XRD, DTG and SEM. Accordingly, the result revealed that, under 90-days of moist curing, the key minerals detected in gypseous kaolin stabilised with calcium-based stabiliser are kaolinite, calcium silicate hydrate, portlandite, and ettringite, whereas only kaolinite, gypsum, brucite and magnesium silicate hydrate were detected in gypseous kaolin stabilised with magnesium oxide. However, under 200-days of water soaking period, no trace of gypsum, ettringite and portlandite were detected in the XRD of 10L- and 10C-based specimens, accompanied by the indication of new minerals (hemihydrate, anhydrite, calcite, and aragonite), suggesting the carbonation of ettringite during the soaking in water.

Keywords: (Ettringite, sulfate, ettringite carbonation, lime, Portland cement, magnesium oxide)

Introduction

Stabilisation of expansive soils with hydraulic stabilisers (Portland cement, lime, and magnesium oxide) has been a promising treatment technique for improving the physico-mechanical characteristics and reducing the swell-shrink attitude of expansive soil under moisture fluctuations [1]. The cement-induced improvement is typically assigned to the cement hydration; a basic reaction involved the dissolution of C_3S, C_3A, C_2S, and C_4AF, with the formation, by precipitation, of calcium silicate hydrate (C-S-H), calcium aluminate hydrate (C-A-H) and calcium hydroxide (CH, also called portlandite) [2]. These hydrates crystalline with time, binding/interlocking the host soil mixture and improving plasticity index [3], shear strength [4], compressive strength [5], robustness against freezing and thawing [5-6], and the swelling behaviour of the soil [7], As for the improvement induced by lime and magnesium oxide, this essentially occurs due to two basic sets of reaction mechanisms: one being shorth-term reactions (cation exchange and flocculation of soil particles) while the second is a long-term reaction (pozzolanic reaction). Upon the addition of quicklime (calcium oxide) and magnesium oxide to the soil in the existence of moisture, the quicklime initially hydrated to calcium hydroxide and then dissolved releasing calcium ions and hydroxyl ions [8], in line with equations 1-to-2. As for the

magnesium oxide, it gets protonated by H+ ions and then the magnesium oxide precipitates [9], in line with equations 3-to-6.

$$CaO+H_2O \rightarrow Ca(OH)_2+\uparrow heat \ldots\ldots\ldots\ldots(1)$$

$$Ca(OH)_2 \rightarrow Ca^{2+} + 2OH^- \ldots\ldots\ldots\ldots\ldots\ldots(2)$$

$$MgO + H_2O \rightarrow MgOH^+_{(surface)} + OH^-_{(aqueous)} \ldots(3)$$

$$MgOH^+_{(surface)} + OH^-_{(aqueous)} \rightarrow MgOH^+ \cdot OH^- \ldots\ldots(4)$$

$$MgOH^+ \cdot OH^-_{(surface)} \rightarrow Mg^{2+} + 2OH^-_{(aqueous)} \ldots\ldots(5)$$

$$Mg^{2+} + 2OH^-_{(aqueous)} \rightarrow Mg(OH)_{2\,(solid)} \ldots\ldots\ldots(6)$$

These reactions, therefore, cause the cation exchange on the soil particles, and such a replacement in cations occurs in the order of $Na^+ < K^+ < Mg^{++} < Ca^{++}$, in which higher valence cations replace those of lower valence cations [8]. This ions substitution balances the electronic charge of the soil particles, induces flocculation-agglomeration of soil particles [10], and promotes different soil particle arrangements [11]. Besides, the hydroxide ions (OH) cause a significant increase in the alkalinity (pH) value (>10), aiding the octahedral and tetrahedral sheets of soil particles to release silica and alumina ions [12]. Thereafter, this initiates the pozzolanic reactions, forming hydrates such as CSH, and CAH in the case of lime [10], and magnesium silicate hydrate (MSH) in the case of magnesium oxide [13-16], all of which enable the interlocking of the system and improving the physico-mechanical chractaristics of the soil. Portlandite (calcium hydroxide) and brucite may also remain from the interaction between the binder and soil if a surplus binder content was provided. This surplus binder coats the particles, delaying the dissolution of soil particles and the pozzolanic reaction, as well as reducing the cohesion of the soil matrix [17-18].

In the attendance of gypsum, however, the calcium-based stabiliser reaction mechanisms are altered due to the nucleation of highly hydrated mineral in the form of needles- and rod-shaped crystals in line with equation 7, known as ettringite [19], owing to the interaction between calcium, alumina, and sulfate in the existence of water.

$$6Ca^{2+} + 2Al(OH)_4^- + 4OH^- + 3(SO_4)^{2-} + 26H_2O$$

$$\rightarrow Ca_6[Al(OH)_6]_2 \cdot (SO_4)_3 \cdot 26H_2O \ldots\ldots\ldots\ldots(7)$$

The ettringite is a problematic issue from a soil stabilisation point of view, as it has a higher water absorption, thus facilitating the volume increase of the host matrix [20]. The ettringite also occurs in a complex mechanism and of dependence on the mineralogy of soil, binder composition, moisture content, temperature and so on. Therefore, researchers use multi-scale analytical investigations such as XRD, DTG, and SEM analysis among others, to quantify the amount of formed ettringite within the stabilised soil mixture for deeper understanding of the reaction mechanisms.

In this context, Puppala et al., (2005) [21], conducted a laboratory investigation using both XRD and SEM and reported that calcium oxide produces both crystalline ettringite and calcite, of which the latter seems to act as a seeding or templating material promoting the formation of calcite over the formation of ettringite. Aldaood et al., (2014) [22], detected the ettringite reflections in the XRD of UCS kaolin samples treated with 3% of lime and containing gypsum content of ≥ 5%, of which the intensity of ettringite reflections was increased as the curing period and temperature increase.

However, in some cases, the detection of ettringite crystals is difficult particularly in the case of the XRD pattern after completion of the expansion, suggesting the appearance of ettringite under the microstructure analysis is also dependent on the curing and experimental procedure. For example, Jha and Sivapullaiah (2015) [23], reported no trace of ettringite crystalline in the XRD of gypsum-dosed soil samples dosed with lime and containing sulfate content of up to 6%, although the specimens represent a continues increasing swelling (heaving) trend indicating the formation needles-like ettringite. So, despite the extensive existing research studies, there are still outstanding questions about the appearance of ettringite minerals in stabilised sulfate soils under the microstructure analysis.

In this context, this research study was carried out using a variety of analytical and microstructural investigations including XRD, DTG, and SEM, with a view to identifying the possible rationale for the detection and the absence of ettringite under these tests.

Methodology

1- Materials

The raw ingredients utilized during the laboratory experimentations included kaolin soil (K), gypsum (G), Portland cement (C), lime (L), magnesium oxide (M), and deionized water. **Table 1** and **Table 2** outline the main oxide charactaristics and physical charactaristics of the raw materials, respectively, whereas **Fig.1** and **Fig.2** plot the sieve analysis curves and the DTG curves curves of the raw ingredients.

Table 1: Oxide properties of raw ingredients.

Oxides	K	C	L	M
CaO	0.01	61.5	71.6	-
MgO	0.21	3.54	0.58	>98
SiO_2	47.3	18.8	0.67	-
Al_2O_3	35.9	4.77	0.07	-
Na_2O	0.07	0.02	0.02	-
P_2O_5	0.12	0.1	0.03	-
Fe_2O_3	0.69	2.87	0.05	-
Mn_2O_3	0.02	0.05	0.02	-
K_2O	1.8	0.57	0.01	-
TiO_2	0.02	0.26	0.01	-
V_2O_5	0.01	0.06	0.02	-
BaO	0.07	0.05	0.01	-
SO_3	0.01	3.12	0.19	-
LOI	0.1	4.3	27.4	-

Table 2: Physical charactaristics of kaolin, Portland cement, lime, and magnesium oxide.

Properties	K	C	L	M
Density (kg/m^3)	-	1400	480	-
Particle density(Mg/m^3)	2.14	3.15	2.8	3.58
pH Value	5.37	13.41	12.6	11.90
Colour	White	Grey	White	White

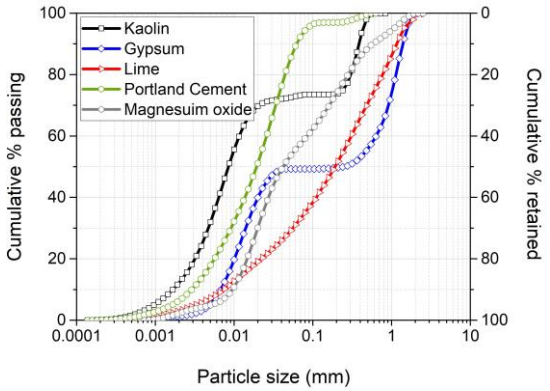

Fig.1: Sieve analysis curves of kaolin, gypsum, lime, Portland cement and magnesium oxide.

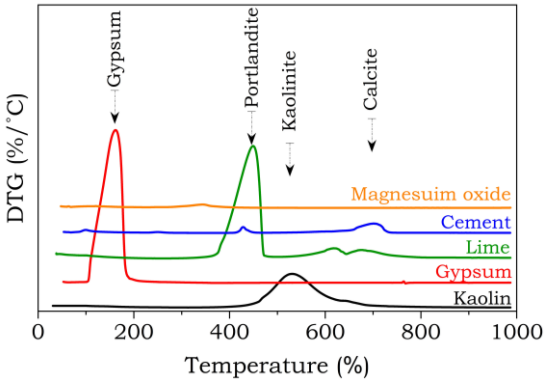

Fig.2: Derivative thermogravimetric (DTG) of raw materials.

The kaolin (K) used was a semi-processed kaolin soil with a liquid limit, plastic limit, and plasticity index of 56.7%, 33.3%, and 23.4%, respectively; it was sourced from Potterycrafts Ltd, Stoke-on-Trent, UK. The DTG curve (see **Fig.2**) revealed a major endothermic peak at 400-700°C because of the decomposition of kaolinite minerals [24].

The gypsum (G) utilised was a calcium sulfate dihydrate with a white form; it was obtained from Fisher Scientific Ltd, Loughborough, Leicestershire, UK. The DTG curve (see **Fig.2**) revealed a major endothermic peak at a temperature range of 100-200°C because of the dehydration of the moisture of gypsum [25], confirming the purity of the product.

The cement (C) utilised was a commercially available CEM-I Portland cement with a grey powder texture; it was produced in line with BS EN 197-1: 2011 [26], and supplied by Large Cement, UK. The DTG curve (see **Fig.2**) revealed two major endothermic peaks; the first peak at a temperature of 400-500°C due to the dehydroxylation of portlandite; and the second peak at 650-750°C due to the decomposition of calcite [27].

The lime (L) utilised was a quicklime with an off-white texture: it was sourced from Tarmac Cement and Lime Company, Derby, UK. The DTG (see **Fig.2**) revealed two main endothermic peaks; sharp peak at a temperature of 350-500°C because of the decomposition of quicklime and weaker peak at a temperature of 550-750°C owing to the de-carbonation of calcite [25].

The magnesium oxide (M) used was a commercial reactive magnesia with a white powder texture; it was gotten from Fisher Scientific Ltd, Leicestershire, UK. The DTG curve (see **Fig.2**) revealed a straight flat line without any endothermic peaks.

2- Mix proportions

The mixes (see **Table 3**) evaluated during the experimentations were designed using; 1) two soil materials (industrial kaolin and gypseous kaolin soil); 2) three different binders (Portland cement, lime, and magnesium oxide); and 3) fixed moisture content of 31%. For clarity, the mix design code contains kaolin (K), gypsum (G) and the binder (C for Portland cement, L for lime or M for magnesium oxide), of which G, C, L and M proceeded by a number, representing the solid amount. The G content shown in the designation code denotes the gypsum percentage by the total mass of the artificially gypseous kaolin, whereas the stabiliser amount represents the sabiliser dosage by the total mass of the dry soil. The purpose of designing these mix compositions was to investigate the microstructure of soil stabilization using L, C, and M in the presence and absence of sulfate. As for the adoption of 31 % moisture content (MC), which was equal to 1.1 of the corresponding standard proctor optimum condition, it was because the soil is always compacted wet of moisture to accommodate any moisture losses. In addition, it was not found necessary to establish the optimum moisture content (OMC) for each system due to the time-consuming nature of proctor test and the impracticability of establishing the OMC for each mix [25].

Table 3: Mix compositions of kaolin specimens made with L, C and M at a constant stabiliser content of 10 % by the total weight of the soil.

Design code	Target soil materials (%)		MC	Binder in % by target soil material		
	K	G		L	C	M
K0G-10L	100	0	31	10		
K0G-10C	100	0	31		10	
K0G-10M	100	0	31			10
K9G-10L	91	9	31	10		
K9G-10C	91	9	31		10	
K9G-10M	91	9	31			10

3- Specimen preparation

A total of two stabilized pure kaolin specimens and six stabilized gypseous specimens were fabricated for each mix; 1) two samples were cured in a sealed plastice container for a period of 7-days of moist curing and then used for the DTG analysis; 2) two samples were cured in a sealed plastic container for a period of 90-days of moist curing and then used for the XRD analysis; and 3) two samples were cured in a sealed plastic container for 7 days before being soaked in water for a period 200-days and then tested using XRD and SEM analysis. For each specimen, enough dry ingredients for fabricating a sample with a diameter of 50 mm and height of 100 mm, were mixed using a mixer for 3 minutes. Hereafter, the predetermined moisture content was added, and the mixing was restarted and continued for exra three minutes. Consequently, the mixture was filled into a steel mould and compacted using a jack in aid of a steel frame as detailed elsewhere [20]. Therefore, the specimens were extruded using a plunger, covered with a cling film, and stored in a plastic container, allowing for moist curing until the testing date. At the end of 7 days, the upper and bottom 10mm-part of two specimens were unwrapped and soaked in water for 200 days using a similar procedure used elsewhere [20], for swelling.

4- Testing method

The analytical and microstructure tests adopted in this research study included DTG, XRD and SEM analysis. Prior to testing, the specimens were fractured and dried in a desiccator at 40 ◦C, milled, sieved through a 0.074 mm sieve, and stored in a plastice bottle at 20 ∓ 2 ◦C, preparing for the tests. Thereafter, the DTG analysis was carried out at 7 days of moist curing. The DTG analysis was run from 20 ∓ 2 up to 1000 ℃, at a flow heating ratio of 20 ℃/min and under an argon environment using a TGA55 kit. The XRD was operated using an STOE powder diffraction system at 90 days of moist curing and after 200 days of soaking in water. The XRD analysis was run at a wavelength (λ) of 1.540598 Å, a step size of 0.015°, and an angle scan in the range of 10 to 84. The microstructure analysis was inspected at 200 days of soaking in water, using JSM-7900F scanning electron microscopy (SEM) at an accelerating voltage of 5 kV and magnifications up to 30000x.

Results and discussion

1- Derivative thermogravimetric (DTG).

The DTG curves of pure kaolin samples (K0G) and gypseous kaolin samples (K9G) stabilised with 10L, 10C and 10M at 7-days of moist curing period, are shown in **Fig. 3**.

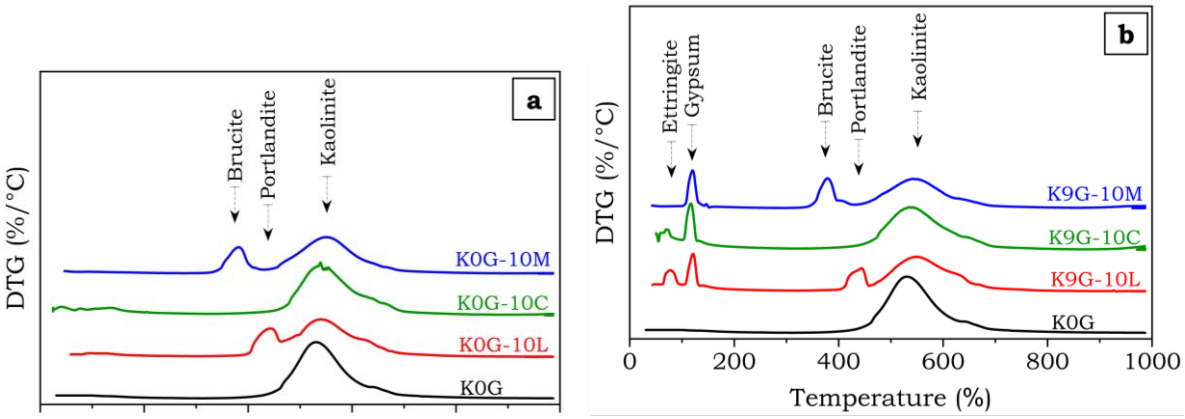

Fig.3: The DTG curves of **a)** kaolin samples and **b)** gypseous kaolin samples, made with 10L, 10C and 10M after 7 days of moist curing.

In the absence of sulfate (K0G), the specimen revealed the presence of a major endothermic peak at 400-700°C pertained to the decomposition of kaolinite [24]. On the use of 10L, 10C, and 10M for stabilisation of pure kaolin (K9G-10L), the DTG analysis exhibited two additional peaks; 1) the first at 350-450°C owing to the decomposition of brucite [28]; and 2) the second peak at 400-500°C due to the decomposition of portlandite [20]. The presence of brucite and portlandite is an indication of the incomplete consumption of binder through the cation exchange, flocculation, and agglomeration of soil particles [28]. However, in the presence of sulfate (K9G), the DTG analysis exhibited two further peaks; 1) the first peak at 50-100°C due to the dehydration of ettringite minerals [20]; and 2) the second peak at a temperature range of 100-200°C due to the dehydration of gypsum [25]. By comparing the height of ettringite peaks, it was apparent that the ettringite mineral was only formed in gypseous kaolin specimens stabilized with a calcium-based stabilizer, and such a mineral was more pronounced in the case of K9G-10L. This was confirmed by the higher gypsum peak, both of which are in support of why calcium-based stabilizers normally yield a superior UCS through soil stabilisation in the presence of sulfate. Apart from ettringite and gypsum peaks, portlandite and brucite peaks were also detected in K9G-10L and K9G-10M, respectively, indicating the incomplete consumption of lime and magnesium oxide used through the fabric modification, which in turn indicates the surplus of both binders. This surplus binder content is not favourable, as it restricts the dissolution of soil particles, delays the pozzolanic reactions, and reduces the cohesion of the system [20]. Therefore, this is in partial support of why 10L induces lower UCS performance in previous study [20].

3- XRD analysis

Fig.4 presents the comparative XRD pattrens of kaolin samples treated with 10L, 10C and 10M after 90 days of moist curing, denoted as M, and after 200 days of water soaking, denoted as S).

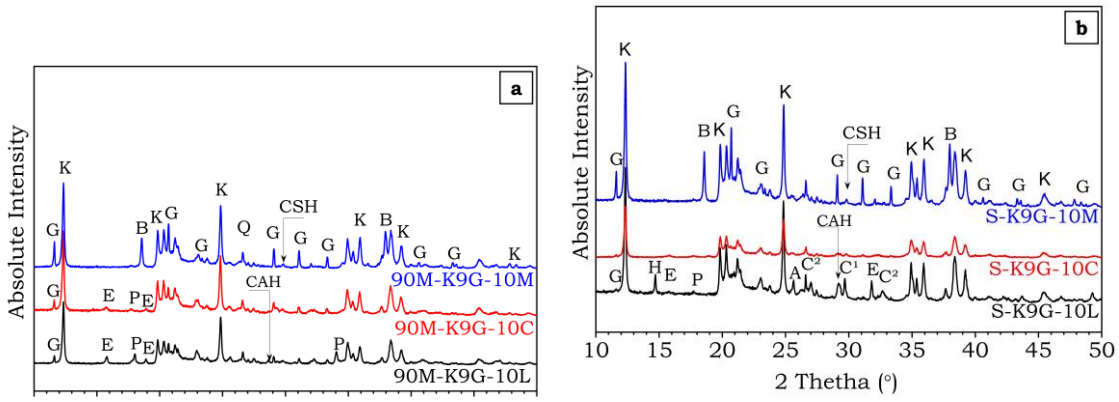

Fig.4: The XRD pattrens of gypseous kaolin treated with 10L, 10C, and 10M at **a)** 90 days of moist curing and **b)** 200-days of water soaking.

After 90-days of moist curing, the primary minerals identified in the XRD patterns were kaolinite-K, gypsum-G, quartz-Q, ettringite-E, portlandite-P, brucite-B, CSH, and CAH. The peak of quartz at $2\theta = 26.6^{\circ}$ appeared to be stable in all the XRD pattrens, whereas the portlandite at $2\theta = 18.08^{\circ}$ was appeared in the 10L-based and 10C-based specimens, with a sharper intensity in the case of the 10L-based specimen, the appreance of which indicates the surplus supply of lime and the incomplete consumption of lime. Similarly, the ettringite peaks at $2\theta = 15.7^{\circ}$ and 18.8° were only detected in 10L-based and 10C-based specimens with a sharper intensity in the case of 10L-based specimens. This was coupled with a reversal order for the gypsum peaks $2\theta = 11.7^{\circ}, 20.7^{\circ}, 23.4^{\circ}, 29.1^{\circ}, 31.1^{\circ}$ and 48.2°, where the gypsum peaks appeared sharper in the 10M-based system, relatively low in the 10L-based specimen, and almost disappeared in the 10L-based specimen, the appearance of which suggests the partial gypsum consumption through the formation and growth of ettringite in the case of 10L and 10C.

In contrast, the brucite peak at $2\theta = 26.6^{\circ}$ was only detected in the 10M-based specimen, which also suggests the surplus supply of magnesium oxide within the system. As for the hydrated products, the CAH at $2\theta = 28.6^{\circ}$ was detected only in 10L-based specimen, whereas the CSH $2\theta = 29.2^{\circ}$ was detected with a hardly visible peak in all the x-ray diffractograms, the appearance of which is most likely because of the overlapping with other minerals. However, during the water soaking, the x-ray diffractograms of gypseous kaolin specimens exhibited considerable micro-structural changes. In this context, a hardly visible trace of portlandite in 10L-based specimens and no trace of portlandite in the 10C-based pattren were detected. This demonstrates the importance of both moisture content and the curing age in the complete consumption of lime. Traces of gypsum peaks in 10L-based and 10C-based diffractograms also disappeared. This disappearance is probably attributed to the presence of water molecules due to the change of curing from moist curing to soaking in water, which eases the solubilization of gypsum and become a source of ions source at the formation sites of the ettringite. As for the ettringite peaks, the x-ray diffractograms exhibited a reduction in the trace of ettringite peaks at $2\theta = 15.7^{\circ}$ and 18.8° to the background, although it appeared at $2\theta = 32^{\circ}$. The disappearance of ettringite is possibly due to the carbonation of ettringite under water soaking condition. This justification was also reinforced by the appearance of new minerals such as hemihydrate (bassanite)-H

at $2\theta = 14.6^{\circ}$ [29-30], in line with [31], and anhydrite-A at $2\theta = 25.6^{\circ}$, as well as some calcium carbonates in the form of calcite (C^1) at $2\theta = 29.2^{\circ}$, and aragonite (C^2) at $2\theta = 27$ and 32.7°. This is also in support of why the ettringite peaks under the XRD were not detected by [21] and [23].

4- SEM analysis

Fig.5 shows the morphology of gypseous kaolin samples made with 10L, 10C, and 10M at 200 days of water soaking. Accordingly, the SEM images exhibited the presence of plate-like kaolinite minerals, needle-like structures, and some small globular-like particles. In the absence of EDS, the only change that can be visualized is the difference in terms of the morphology of hydrats and ettringite minerals. The globular-like particles of the hydrates in the 10L-based system possessed a clumped cluster form with no defined shapes, whereas such hydrates appeared in a well-distributed form in the case of the 10C-based and 10M-based systems. This difference can be assigned to the fineness of both cement and magnesium oxide and the richness of cement with the main oxides needed for the formation of hydrates, both of which promote the distribution of the binder within the system, and thus, facilitates the formation of less clumped hydrates on the edge of soil particles. As for the ettringite, the SEM images revealed the formation of massive ettringite in the case of the 10C-based system with a thicker diameter, relative to that of small and thinner morphology for needles-like prisms formed in the 10L-based system.

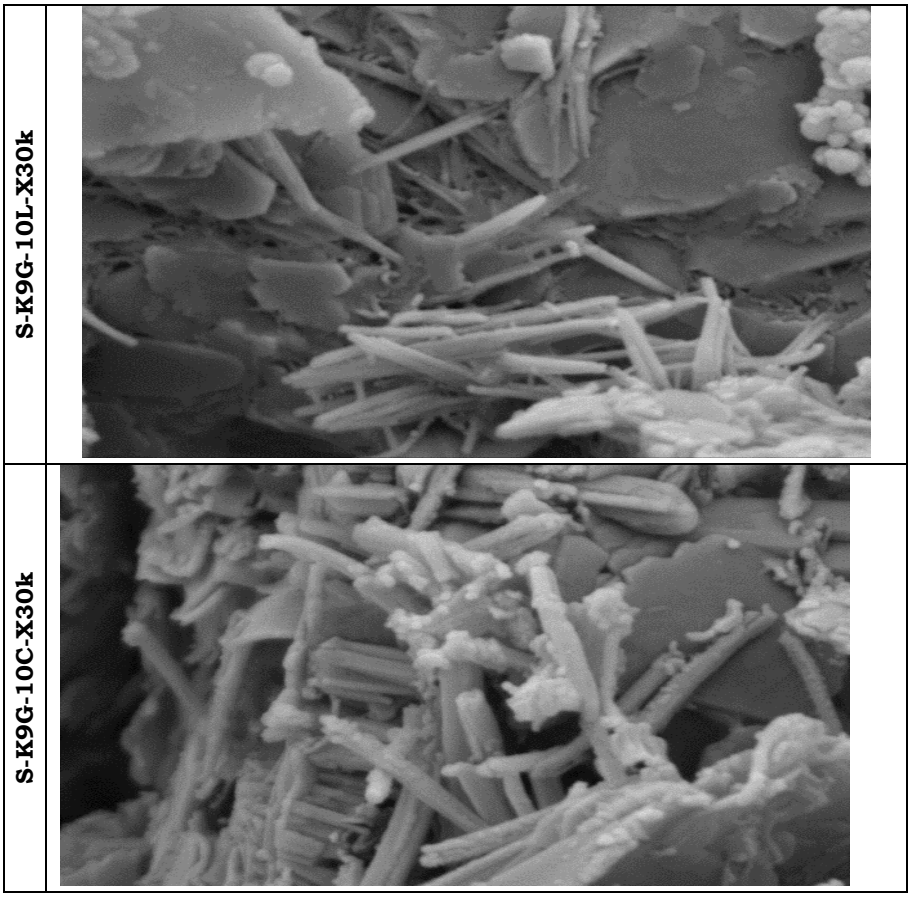

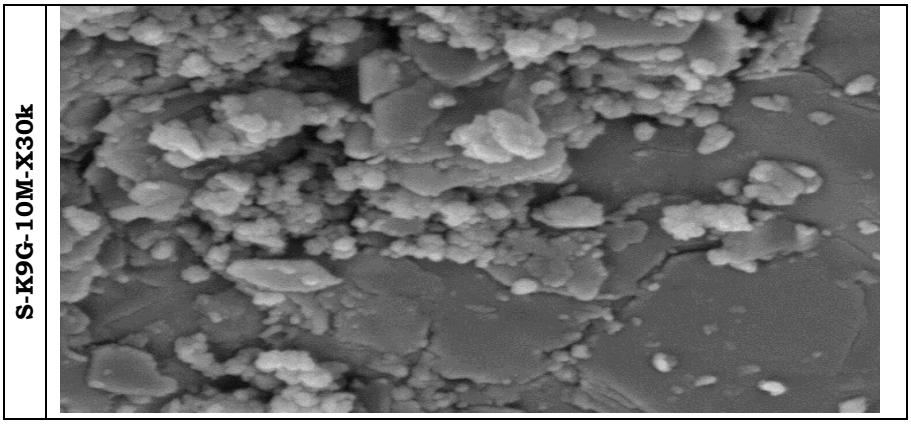

Fig.5: The SEM images of gypseous kaolin samples made with 10L, 10C, and 10M at 200 days of soaking in water.

In theory, the ettrgnite minerals should not be as massive as that of 10L-based cement since cement promotes less calcium hydroxide during hydration [28]. However, because of the faster cement hydration and hardening, and the subsequent restriction of cracks at early curing age, which all tighter inhibit the possibility of carbonation of ettringite within the system, the microstructure morphology obtained here in this study is logical. The thinner ettringite crystals in the 10L-based specimen are also in support of the ettringite carbonation detected in the XRD diffractogram of K9G-10L.

Conclusions

The main conclusions of the analytical and microstructure investigations of this research study are outlined as follows:

The DTG and XRD analysis revealed the existence of portlandite, CSH and CAH in pure kaolin specimen stabilised with 10L and 10C, whereas only brucite was detected in the DTG of pure kaolin specimen stabilised with 10M, the presence of which indicates the surplus supply of the binder.

In the presence of sulfate, all the analytical tests exhibited the nucleation of ettringite in samples treated with L and C, and such minerals seemed to be carbonated under water soaking, forming new minerals such as hemihydrate, anhydrite, calcite, and aragonite.

The main advantage of this research study is the conduction of comprehensive analytical and microstructure tests on sulfate soil stabilised with different binders, facilitating the exploration of a scientific rationale for the absance of ettringite traces in the XRD of gypseous soil treated with L and C, which in turn fills the knowledge gap.

The limitations of this research that could have an influence on the authenticity of the outcomes of the experimentations are the utilisation of an artificially gypseous soil, one source of sulfate (gypsum), and a fixed binder content of 10%. Hence, research studies simulating different sources of sulfate such as magnesium sulfate and sodium sulfate, as well as different binder contents, are recommended to overcome this deficiency.

Overall, it can be inferred that the utilization of Portland cement, lime, and magnesium oxide as a soil stabiliser in the absence of sulfate, is a promising technique. However, only magnesium oxide was effective in the presence of sulfate due to the restriction of ettringite.

Abbreviations and Acronyms

XRD: x-ray diffraction,

DTG: derivative thermogravimetric,

SEM: scanning electron microscopy,

K: kaolin,

G: gypsum,

L: lime,

C: Portland cment,

M: magnesium oxide,

C_3S: Tricacluim silicate,

C_3A: Tricacluim aluminate,

C_2S: Diacalcuim silicate,

C_4AF: Tetracacluim aluminoferrite,

90M: 90 days of moist curing,

S: Soakiing in water for 200 days,

CSH: calcium silicate hydrate,

MSH: magnesium silicate hydrate,

CAH: calcium aluminate hydrate

CH: calcium hydroxide,

Na^{+}: sodium

K^{+}: potassium

Mg^{++}: magnesium

Ca^{++}: clacuim

B: brucite,

P: portalandite,

E: ettrnigte,

C^{1}: calcite,

C^{2}: aragonite,

A: anhydrite,

H: hemihydrate,

Acknowledgement

The authors would like to acknowledge the Advanced Materials Testing Centre (AMTsC), within the School of Engineering at the University of South Wales, for the continuous support during the implementation of the laboratory experimentations.

References

[1] Al-Atroush, M.E., and Sebaey, T.A., (2021), Stabilization of expansive soil using hydrophobic polyurethane foam: A review., Transportation Geotechnics., **27**, 100494. DOI: 10.1016/j.trgeo.2020.100494.

[2] Millán-Corrales, G., González-López, J.R., Palomo, A., and Fernandez-Jiménez, A., (2020), Replacing fly ash with limestone dust in hybrid cements., Construction and Building Materials., **243**, 118169. DOI: 10.1016/j.conbuildmat.2020.118169.

[3] Nigam, S.K., Sinha, A.K., and Madan, S.K., (2023), Characterisation of stabilised red mud waste material for road infrastructure., Materials Today: Proceedings. DOI: 10.1016/j.matpr.2023.06.229.

[4] Salehi, M., Bayat, M., Saadat, M., and Nasri, M., (2023), Prediction of unconfined compressive strength and California bearing capacity of cement-or lime-pozzolan-stabilised soil admixed with crushed stone waste., Geomechanics and Geoengineering., **18**(4), 272-283. DOI: 10.1080/17486025.2022.2040606.

[5] Chenarboni, H.A., Lajevardi, S.H., MolaAbasi, H., and Zeighami, E., (2021), The effect of zeolite and cement stabilization on the mechanical behavior of expansive soils., Construction and Building Materials., **272**, p.121630. DOI: 10.1016/j.conbuildmat.2020.121630.

[6] Orazi, M., Orazi, U.S., Romeo, E., Van Rompaey, G., and Tebaldi, G., (2023), Mechanical recovery of lime-stabilised clays subjected to freeze–thaw damage., Road Materials and Pavement Design., 24(8), pp.2104-2112. DOI: 10.1080/14680629.2022.2117070.

[7] Saleem, A., ur Rehman, Z., Qamar, S., Katubi, K.M., Khan, A.H., Akhtar, M.N., Qamar, N., Alrowaili, Z.A., Saeed, U., Ullah, S., and Assiri, M.A., (2023), Investigations of graphene oxides and cement on strength performance of soil., Journal of Building Engineering., **73**, 106857. DOI: 10.1016/j.jobe.2023.106857.

[8] Jeremiah, J.J., Abbey, S.J., Booth, C.A., and Kashyap, A., (2023), Behaviour and Microstructural Characteristics of Lime-GGBS-Treated Kaolin Clay Contaminated with Gypsum., Materials, **16**(2), 874. DOI: 10.3390/ma16020874.

[9] Park, S., Ma, J., Yun, T.S., Jeon, S., Byeun, Y., Kang, D., and Jang, J., (2020), Pore-scale swelling mechanism of magnesium oxide granules during hydration., Construction and Building Materials., **251**, 119101. DOI: 10.1016/j.conbuildmat.2020.119101.

[10] Vitale, E., Deneele, D., Russo, G., and Ouvrard, G., (2016), Short-term effects on physical properties of lime treated kaolin., Applied Clay Science., **132**, 223-231. DOI: 10.1016/j.clay.2016.04.025.

[11] Pallanza, A., To, P., and Matheson, M., (2023), Lime stabilised road batters: A laboratory simulation of site flood conditions using a customised erosion apparatus and sample digitisation., Transportation Geotechnics., **40**, 100975. DOI: 10.1016/j.trgeo.2023.100975.

[12] Kinuthia, J.M., and Nidzam, R.M., (2011), Towards zero industrial waste: Utilisation of brick dust waste in sustainable construction., Waste Management., **31**(8), 1867-1878. DOI: 10.1016/j.wasman.2011.03.020.

[13] Seco, A., Del Castillo, J.M., Espuelas, S., Marcelino, S., and García, B., (2022), Sulphate soil stabilisation with magnesium binders for road subgrade construction., International Journal of Pavement Engineering., **23**(6), 1840-1850. DOI: 10.1080/10298436.2020.1825711.

[14] Xu, B., and Yi, Y., (2022), Stabilisation/solidification of lead-contaminated soil by using ladle furnace slag and carbon dioxide., Soils and Foundations, 62(5), 101205. DOI: 10.1016/j.sandf.2022.101205.

[15] Seco, A., Miqueleiz, L., Prieto, E., Marcelino, S., García, B., and Urmeneta, P., (2017), Sulfate soils stabilization with magnesium-based binders., Applied Clay Science., **135**, 457-464. DOI: 10.1016/j.clay.2016.10.033.

[16] Li, W., Yi, Y., and Puppala, A.J., (2020), Suppressing ettringite-induced swelling of gypseous soil by using magnesia-activated ground granulated blast-furnace slag., Journal of Geotechnical and Geoenvironmental Engineering., **146**(7), 06020008. DOI: 10.1061/(asce)gt.1943-5606.0002292.

[17] Chemeda, Y.C., Deneele, D. and Ouvrard, G., (2018), Short-term lime solution-kaolinite interfacial chemistry and its effect on long-term pozzolanic activity., Applied Clay Science., **161**, 419-426. DOI: 10.1016/j.clay.2018.05.005.

[18] Choobbasti, A.J., and Kutanaei, S.S., (2017), Microstructure characteristics of cement-stabilized sandy soil using nanosilica., Journal of Rock Mechanics and Geotechnical Engineering., **9**(5), 981-988. DOI: 10.1016/j.jrmge.2017.03.015.

[19] Kinuthia, J.M. and Wild, S., (2001), Effects of some metal sulfates on the strength and swelling properties of lime-stabilised kaolinite., International Journal of Pavement Engineering., **2**(2), 103-120. DOI: 10.1080/10298430108901720.

[20] Ebailila, M., Kinuthia, J., and Oti, J., (2022), Suppression of Sulfate-Induced Expansion with Lime–Silica Fume Blends., Materials., **15**(8), 2821. DOI: 10.3390/ma15082821.

[21] Puppala, A.J., Intharasombat, N., and Vempati, R.K., (2005), Experimental studies on ettringite-induced heaving in soils., Journal of Geotechnical and Geoenvironmental Engineering., **131**(3), 325-337. DOI: 10.1061/ASCE1090-02412005131:3325.

[22] Aldaood, A., Bouasker, M., and Al-Mukhtar, M., (2014), Free swell potential of lime-treated gypseous soil., Applied Clay Science., **102**, 93-103. DOI: 10.1016/j.clay.2014.10.015.

[23] Jha, A.K., and Sivapullaiah, P.V., (2016), Volume change behavior of lime treated gypseous soil—influence of mineralogy and microstructure., Applied Clay Science., **119**, pp.202-212. DOI: 10.1016/j.clay.2015.09.017.

[24] Al-Mukhtar, M., Lasledj, A., and Alcover, J.F., (2014), Lime consumption of different clayey soils., Applied Clay Science., **95**, 133-145. DOI: 10.1016/j.clay.2014.03.024.

[25] Ebailila, M., Kinuthia, J., and Oti, J., (2022), Role of Gypsum Content on the Long-Term Performance of Lime-Stabilised Soil., Materials., **15**(15), 5099. DOI: 10.3390/ma15155099.

[26] BS EN 197-1:2011, Cement — Part 1: Composition, specifications and conformity criteria for common cements, BSI Standards Limited, London, UK, 2011. https://doi.org/10.3403/30205527.

[27] Adeleke, B.O., Kinuthia, J.M., Oti, J., and Ebailila, M., (2023), Physico-mechanical evaluation of geopolymer concrete activated by sodium hydroxide and silica fume-synthesised sodium silicate solution., Materials., **16**(6), 2400. DOI: 10.3390/ma16062400.

[28] M. Ebailila, Sulfate soil stabilisation with silica fume-based binders, Doctoral Thesis, University of South Wales, England, UK, 2022.

[29] Vakili, M.V., Chegenizadeh, A., Nikraz, H., and Keramatikerman, M., (2016), Investigation on shear strength of stabilised clay using cement, sodium silicate and slag., Applied Clay Science., **124**, 243-251. DOI: 10.1016/j.clay.2016.02.019.

[30] Ahmed, A., (2015), Compressive strength and microstructure of soft clay soil stabilized with recycled bassanite., Applied clay science., **104**, 27-35. DOI: 10.1016/j.clay.2014.11.031.

[31] Aldaood, A., Bouasker, M. and Al-Mukhtar, M., (2014), Impact of wetting–drying cycles on the microstructure and mechanical properties of lime-stabilized gypseous soils., Engineering Geology., **174**, 11-21. DOI: 10.1016/j.enggeo.2014.03.002.